AGU100 ADVANCING EARTH AND SPACE SCIENCE

Geophysical Research Letters

RESEARCH LETTER
10.1029/2019GL082220

Key Points:
- The surface downward longwave radiation (DLR) response to forcing is determined by surface temperature
- Vertically integrated radiative kernels explain 71–84% of the variance in the DLR response to greenhouse gas forcing
- Changes in cloud cover contribute only 11% of the DLR response to greenhouse gas forcing

Supporting Information:
- Supporting Information S1

Correspondence to:
L. R. Vargas Zeppetello,
lvz7@uw.edu

Citation:
Vargas Zeppetello, L. R., Donohoe, A., & Battisti, D. S. (2019). Does surface temperature respond to or determine downwelling longwave radiation? *Geophysical Research Letters*, *46*, 2781–2789. https://doi.org/10.1029/2019GL082220

Received 30 JAN 2019
Accepted 13 FEB 2019
Accepted article online 19 FEB 2019
Published online 5 MAR 2019

Does Surface Temperature Respond to or Determine Downwelling Longwave Radiation?

L. R. Vargas Zeppetello[1], A. Donohoe[2], and D. S. Battisti[1]

[1]Department of Atmospheric Sciences, University of Washington, Seattle, WA, USA, [2]Polar Science Center, Applied Physics Laboratory, University of Washington, Seattle, WA, USA

Abstract Downward longwave radiation (DLR) is often assumed to be an independent forcing on the surface energy budget in analyses of Arctic warming and land-atmosphere interaction. We use radiative kernels to show that the DLR response to forcing is largely determined by surface temperature perturbations. We develop a method by which vertically integrated versions of the radiative kernels are combined with surface temperature and specific humidity to estimate the surface DLR response to greenhouse forcing. Through a decomposition of the DLR response, we estimate that changes in surface temperature produce at least 63% of the clear-sky DLR response in greenhouse forcing, while the changes associated with clouds account for only 11% of the full-sky DLR response. Our results suggest that surface DLR is tightly coupled to surface temperature; therefore, it cannot be considered an independent component of the surface energy budget.

Plain Language Summary Longwave radiation, often referred to as "thermal" or "infrared" radiation, emitted downward by Earth's atmosphere is a primary contributor to the surface energy budget. Numerous studies have invoked longwave radiation as a driver of surface warming. This paper shows that this line of reasoning fails to account for the strong control surface temperature exerts on longwave radiation. Using radiative kernels, matrices that quantify the longwave radiation response to a climate perturbation (like global warming), we argue that any surface temperature anomaly will generate a downward longwave radiation response. This constitutes a feedback between the Earth's surface and its atmosphere. The kernels show large longwave responses to perturbations in the lowest part of the atmosphere and almost no response to perturbations at high levels; by vertically integrating the kernels, we can ignore the vertical structure of climate perturbations. Using this modification, we predict the longwave radiation response to a warming world using only the surface changes. Our prediction agrees with climate model output, suggesting that the longwave radiation response is determined primarily by surface temperature. Further, the cloud contribution to changes in longwave radiation is small. These results provide clarity on how changes in the surface energy budget should be analyzed.

1. Introduction and Hypothesis

Research on climate feedbacks aims to disentangle the global climate's response to a particular forcing from the impact of the forcing itself. Studies of climate feedbacks have traditionally analyzed model representations of the top of atmosphere (TOA) radiative budget (Bony et al., 2006; Mhyre et al., 2013). Much less attention is given to the surface energy budget due to large observational uncertainties that obscure the distinction between forcing and response (Wild et al., 2013). Despite these observational uncertainties, anthropogenic climate forcing will drive important changes to the surface energy budget. For example, greenhouse warming experiments feature annual mean downward longwave radiation (DLR) increases between 10 and 40 W/m^2 (Stephens et al., 2012); anomalies of the same order of magnitude were observed during the warm Arctic winter of 2015/2016 (Kim & Kim, 2017). It has been hypothesized (Burt et al., 2016; Woods & Caballero, 2016) that Arctic warming can be *caused* by large DLR anomalies. Similarly, studies using offline land models often consider surface DLR as an independent *forcing* on Earth's surface energy budget that can drive surface warming. In this study, we will show that for any process driven by either internal variability or external forcing, the equilibrated DLR response is driven by the surface temperature change.

That DLR is highly sensitive to surface temperature can be inferred from Figure 1a, which shows the zonal mean of the vertical structure for both the temperature and specific humidity kernels. Both kernels have their largest values in the lowest atmospheric layers. We show only the values below 500 hPa because no large values exist above that level in either kernel. Figure 1a strongly suggests that climate perturbations above the boundary layer have a small impact on surface DLR, while changes near the surface are extremely important. The temperature kernel (red colors in Figure 1a) increases monotonically with increasing pressure, indicating that DLR is most sensitive to temperature changes that are closest to the surface. The specific humidity kernel (blue contours in Figure 1a) has values roughly one third those of the temperature kernel, and a local maximum at 925 hPa. Figure 1b shows the zonal mean of the vertically integrated kernels, obtained by summing each grid box in the vertical column. A feedback of more than 5 $W \cdot m^{-2} \cdot K^{-1}$ is found in the tropics, most of it originating below the 850-hPa level. By differentiating the Stephan-Boltzman equation and multiplying the result by an unperturbed zonal mean surface temperature distribution, we compute the Planck feedback that is slightly larger than the DLR feedback (compare solid black and dashed black lines in Figure 1b). The near-blackbody nature of the lower atmosphere suggests a mechanism that connects surface warming with enhanced DLR.

Surface temperature and humidity changes are efficiently communicated throughout the boundary layer by turbulent energy fluxes; as such, the surface and boundary layer temperature respond to forcing in concert and with equal magnitude. Given the lower atmosphere's large DLR sensitivity illustrated by the radiative kernels, we can infer that turbulent fluxes of heat and moisture to the boundary layer will induce a large DLR response whenever a surface temperature anomaly is present. Therefore, any surface temperature anomaly will generate a DLR response; the processes that initiated the surface temperature anomaly—whether internal or forced—is irrelevant. Instead of being considered an independent forcing on the surface, the kernels suggest that DLR responds to surface temperature through efficient boundary layer mixing of heat and moisture.

In section 2, we present two methods for decomposing clear-sky DLR changes into responses to temperature and specific humidity changes; both methods use the radiative kernels. The first method uses the vertical structure of atmospheric temperature and specific humidity perturbations; we refer to this as *the traditional approach*. The second uses only the temperature and specific humidity perturbations at the surface; we refer to this as *the vertically integrated approach*. We then demonstrate that both methods can produce the surface DLR responses to greenhouse warming in an ensemble of models. In section 3, we quantify various contributions to the surface DLR response to greenhouse warming. Section 4 contains a summary and discussion of major results.

2. The Preeminence of the Boundary Layer Control on DLR

A radiative kernel is a matrix that assigns radiative responses to climactic perturbations. For the temperature kernel, the perturbation is a 1° warming, while for the specific humidity kernel, it is the increase in specific humidity associated with a 1° warming under the assumption that relative humidity remains constant everywhere in the atmosphere (see Soden & Held, 2006; Soden et al., 2008). To compliment their TOA cousins, surface radiative kernels have been developed to quantify the response of surface radiation to changes in atmospheric temperature and specific humidity (Pendergrass et al., 2018; Previdi, 2010). In this study, we use the clear- and full-sky temperature and specific humidity kernels from Previdi (2010).

The traditional approach requires three-dimensional climate model output because the vertical structure of climate perturbations is of extreme importance to the TOA radiative response (Hansen et al., 2005). However, the kernels shown in Figure 1a suggest that only the near-surface temperature and specific humidity matter for surface DLR. We test this hypothesis in this section by comparing the changes in surface DLR simulated by climate models in response to greenhouse gas forcing to those estimated from (i) the radiative kernels using the full 3-D temperature and specific humidity changes and from (ii) the vertically integrated kernels assuming temperature and specific humidity changes that are uniform with height and equal to those at the surface.

We analyze the change in surface DLR climatology (ΔDLR) between two 10-year periods (2010–2019 and 2090–2099) of the RCP8.5 global warming scenario in the GFDL-CM3 model. The GFDL-CM3 model was chosen at random, though we intentionally did not analyze output from the ECHAM5 model because it

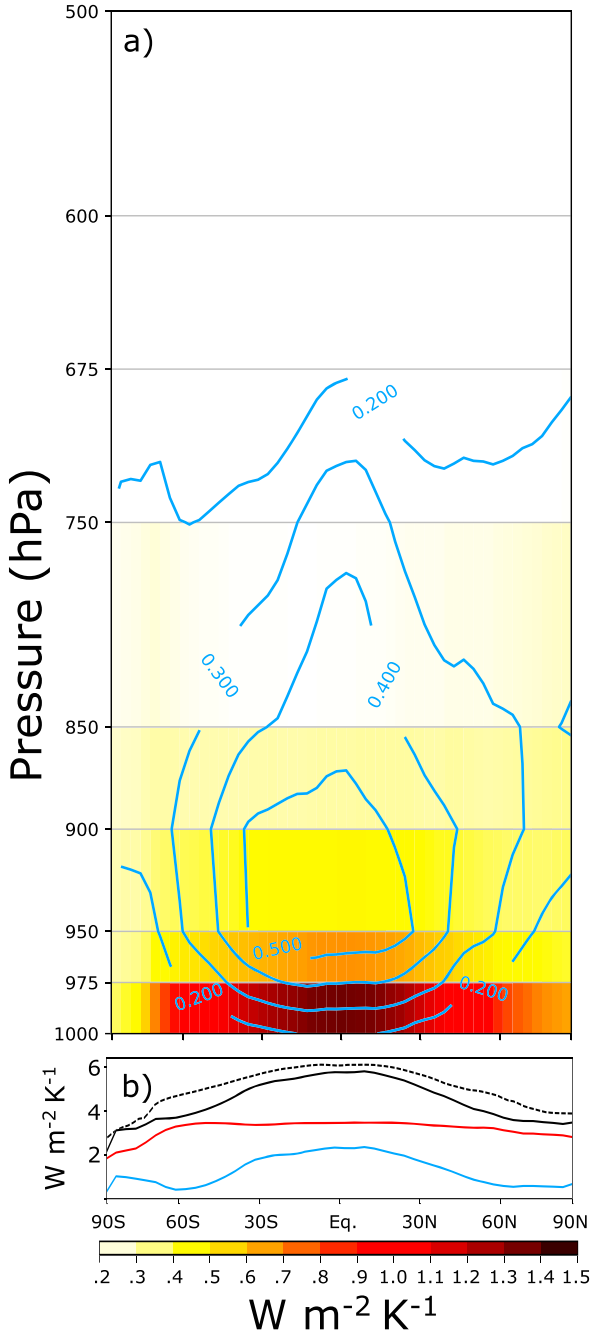

Figure 1. (a) Zonally averaged clear-sky surface radiative kernels for temperature (shading) and specific humidity (contour interval 0.1 $W \cdot m^{-2} \cdot K^{-1}$) as a function of pressure level from Previdi (2010). The specific humidity kernel has been normalized such that values displayed show the longwave radiative response induced by the water vapor equivalent of a 1 K warming under the constant relative humidity assumption. (b) Vertically integrated temperature (red) specific humidity (blue) kernels. Also shown are the sum of the two kernels (solid black) and the Planck feedback (dashed black). A nearly identical figure for the full-sky kernels is shown in Figure A1.

was used to make the Previdi kernels and we wanted to demonstrate the model-independent nature of our hypothesis. Figures S1 and S2 in the supporting information show similar results to those below for four additional models, demonstrating the model-independent nature of our hypothesis. Studies using radiative kernels to evaluate climate feedbacks have verified that they are insensitive to the choice of model (e.g., Held & Shell, 2012; Soden et al., 2008), so we have no reason to believe that extending the analysis to a wider set of models would impact our results.

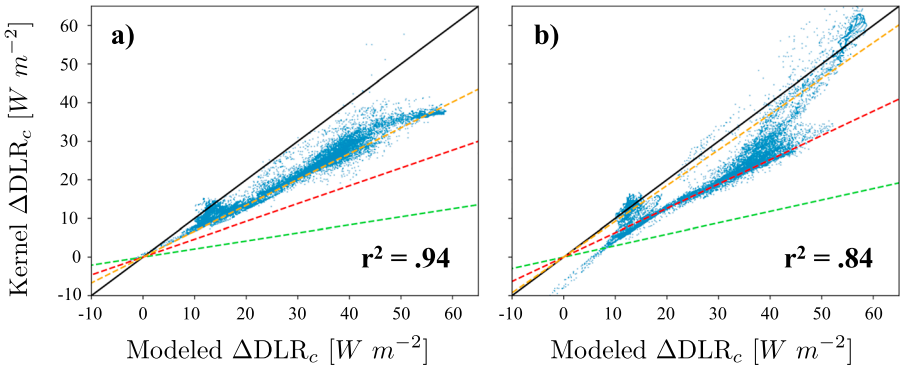

Figure 2. Scatter plots of the change in clear-sky downward longwave radiation (DLR; ΔDLR_c) produced by the (a) traditional and (b) vertically integrated kernels versus the ΔDLR_c modeled by GFDL-CM3. The red dashed lines show regressions of the temperature contributions to ΔDLR_c (equations (A1) and (A2)), while the green dashed lines show regressions of the specific humidity contributions to ΔDLR_c (equations (A3) and (A4)). The orange dashed lines show the sum of the two regressions, while the solid black line is the 1:1 line. The variance explained by each method is shown in the bottom right corner of the plot.

We focus, for now, on the clear-sky DLR response (ΔDLR_c) because there are no kernels to explicitly estimate the cloud contribution. We quantify the cloud contributions to full-sky ΔDLR in section 3. Figure 2a shows a scatter plot of each model grid box's value for ΔDLR_c produced by the traditional kernel method as a function of modeled ΔDLR_c. A linear regression of the temperature component (equation (A1)) is shown with the red dashed line, while an analogous regression of the specific humidity component (equation (A3)) is shown with the green dashed line.

A regression of the total kernel-produced clear-sky ΔDLR_c, given by the sum of the temperature and specific humidity components, is shown in Figure 2a by the dashed orange line, and the solid black line indicates one-to-one correspondence. This regression and the scatter plot both show that ΔDLR_c is underpredicted by the traditional kernel approach. Shell et al. (2008) have argued that correlations between temperature and atmospheric emissivity due to increases in specific humidity could cause the kernel underprediction of ΔDLR_c; we show evidence for this hypothesis in section 3. A doubling in atmospheric CO_2 also contributes to ΔDLR_c, but Andrews et al. (2009) and Colman (2015) found that the CO_2 forcing on surface longwave radiation is at most 1 W/m^2, and observational evidence suggests a trend of only 0.2 W/m^2 per decade from 2000 to 2010 (Feldman et al., 2015). CO_2 forcing is extremely small compared to the DLR response shown in Figure 2, and the fact that the kernel approach does not account for it cannot explain the underprediction. Still, the traditional kernel method explains an impressive 94% of the clear-sky ΔDLR_c variance in GFDL-CM3; we found similar values in two other climate models (see supporting information Figure S1).

The vertical structure of the radiative kernels suggests that only changes in atmospheric temperature and specific humidity at the surface are relevant to surface DLR. To test this hypothesis, we sum the kernel values for the entire atmospheric column over a particular grid box to generate the vertically integrated kernels. The resultant vertically integrated kernels (W·m^{-2}·K^{-1}) represent the DLR adjustment if surface anomalies propagated through the entire atmospheric column. We assume that surface perturbations penetrate through the entire atmosphere, but the supporting information (Figure S3) shows that our results are largely insensitive to the upper integration limit on the vertically integrated kernels, as long as this limit is above the boundary layer. After the integration, we perform the same convolutions from the traditional approach but use the vertically integrated kernels and surface GFDL-CM3 output for temperature and specific humidity.

Figure 2b shows how faithfully the vertically integrated kernels reproduce surface ΔDLR_c in GFDL-CM3, along with the same three linear regressions from Figure 2a. The vertically integrated approach explains 84% of the clear-sky ΔDLR_c variance; similar results are obtained using output from four other climate models (see supporting information Figure S2). While the vertically integrated method generally underpredicts ΔDLR_c, there are some notable overpredictions. These are mainly in the high northern latitudes, where changes in surface temperature are greater than changes in boundary layer temperature due to a near-surface inversion. The polar inversion is known to flip the sign of the lapse rate feedback by trapping

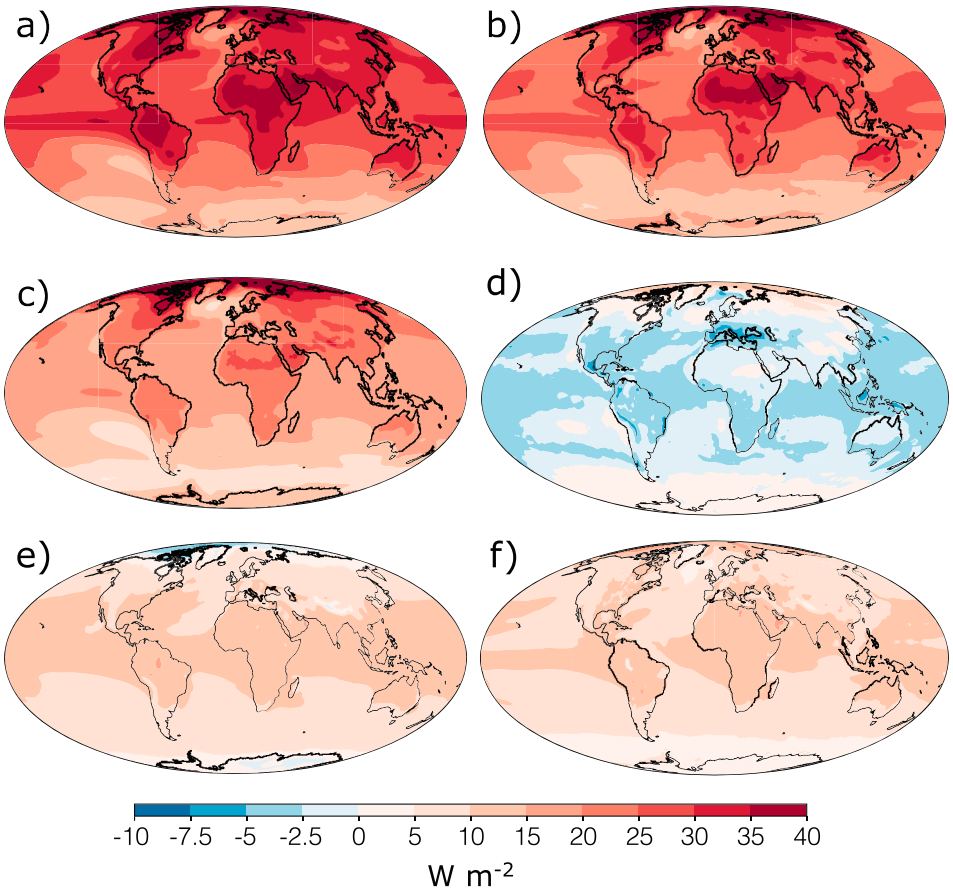

Figure 3. Changes to surface downward longwave radiation (DLR) in the five-model ensemble mean, along with various contributions. Panels (a) and (b) show changes in clear- and full-sky DLR, respectively. Panel (c) shows the change in clear-sky DLR (ΔDLR_c) obtained from the vertically integrated kernel method. Panel (d) shows the cloud contributions to DLR changes (see Appendix A for explanation). Panel (e) shows the difference in ΔDLR_c estimated using the vertically integrated kernels and that simulated by the model: panel (a) minus (c). Panel (f) shows the difference in ΔDLR_c estimated using the traditional kernels and that simulated by the model.

warming near the surface (Colman, 2015; Feldl & Roe, 2013). This biases our vertically integrated method toward overpredicting ΔDLR_c in the Arctic. Still, the agreement between the two scatter plots in Figure 2 validates our hypothesis that most of the DLR response to greenhouse forcing is driven by increases in surface temperature. The supporting information (Figure S4) shows a map of the difference between the vertically integrated and traditional method's prediction of ΔDLR_c that demonstrates their similarity.

3. Sources of the DLR Response to Greenhouse Forcing

We now quantify the surface temperature, specific humidity, and cloud contributions to the DLR response to greenhouse forcing in an ensemble of climate models (for ensemble members, see supporting information Table S1). Figures 3a and 3b show maps of the clear- and full-sky DLR response averaged over our five-member ensemble. Both maps show a large response between the two periods with maximum values in the Arctic of over 40 W/m^2.

Figure 3c shows the DLR_c response produced by convolving the surface changes in temperature and specific humidity with the vertically integrated kernels; it has a similar spatial pattern to the ensemble mean response shown in Figure 3a. While our formulation of the specific humidity component (see equation (A4)) relies on surface specific humidity model output, we combine the two components in Figure 3c and ascribe the surface specific humidity increases to surface warming. Under the fixed relative humidity assumption, changes in specific humidity are purely "thermodynamic" and can be attributed to temperature changes

(Held & Shell, 2012; Held & Soden, 2006). Using temperature changes and the fixed relative humidity assumption to predict the evolution of surface specific humidity introduces a globally averaged difference of 0.92 W/m^2 in the results from Figure 3c (see supporting information Figure S5). Therefore, we assume that surface temperature drives both components; combined, they account for 63% of the globally averaged DLR_c response.

Figure 3e shows the error in the vertically integrated approach given by subtracting Figure 3c from Figure 3a. The error has a strong meridional structure, with the largest kernel underpredictions in the tropics, where Pendergrass et al. (2018) also found the largest errors in surface longwave radiation in their kernel-based study. This is likely due to the correlation between specific humidity and temperature changes that is largest in the hottest, most humid regions. If so, it may be safe to assume that the residual term in Figure 3e should be combined with the surface temperature and specific humidity components, but we will refrain from doing so here. Whatever the source of error, it does not stem from neglecting the vertical structure of the radiative perturbations, as the error structure for the traditional method shown in Figure 3f is almost identical to Figure 3e, with the exception of the vertically integrated method's overprediction associated with polar surface inversions.

Figure 3d shows the cloud component of the surface full-sky DLR response, obtained by taking the difference between the full- and clear-sky ΔDLR model output and removing the effect of cloud masking using the full-sky kernels (see Appendix A). The cloud component is negative everywhere except in the high latitudes where clouds increase DLR slightly. This spatial pattern agrees broadly with the cloud impacts on DLR described in Colman (2015), but importantly, for our driving question, the magnitude of the cloud-induced DLR response is much smaller than the response attributed to surface temperature changes by the radiative kernels. In the global average, the magnitude of the cloud component is roughly 11% of the full-sky DLR response, indicating that clouds play a relatively minor role in the DLR response to greenhouse warming. Colman (2015) found this spatial pattern of cloud feedbacks on surface DLR with a model not used in our analysis using only increases in sea surface temperature associated with CO_2 forcing. Thus, it is possible that some of these cloud changes are associated with increased surface temperature. However, the kernels are not able to definitively attribute the DLR cloud response to temperature or humidity perturbations and we refrain from doing so here. Such an attribution exercise falls outside the scope of this study.

4. Conclusions

In summary, we have presented the surface DLR kernels from Previdi (2010) and argued that the DLR response to greenhouse forcing is controlled primarily by increases in surface temperature. Calculations show that 84% of the variance in ΔDLR_c can be explained using only surface temperature, surface specific humidity, and the vertically integrated kernels. The traditional kernel approach explains 94% of the variance. Hence, very little information on ΔDLR_c is provided by the vertical structure of climate and radiative perturbations. While the kernels reproduce the modeled ΔDLR_c fairly accurately, both approaches have a systemic underprediction likely due to the correlation between temperature and specific humidity. Despite this underprediction, we attribute more than 60% of the predicted DLR_c response in our five-model ensemble to changes in surface temperature under the assumption of fixed relative humidity. The cloud changes account for only 11% of the full-sky DLR response.

We are not arguing that DLR anomalies are incapable of driving surface temperature changes. Warm air intrusions and atmospheric moisture convergence events can certainly generate surface warming by increasing DLR. However, the equilibrated DLR response to *any* forcing will be governed by the surface temperature rather than the forcing (whatever the forcing may be due to, e.g., changes in shortwave, longwave, and albedo). The purely radiative response to an increase in atmospheric CO_2 is instructive: a doubling of atmospheric CO_2 causes a 1-W/m^2 increase in DLR at the surface. After adjustment, the surface temperature increases by 2 °C and the net 1-W/m^2 longwave forcing is balanced by net change in upward longwave of 1 W/m^2 that is accomplished by a (Planck) feedback of 10 W/m^2 and an increased DLR feedback of 9 W/m^2. Of course, in the real world, turbulent energy fluxes (particularly evapotranspiration) compensate for the reduced effectiveness of radiative cooling caused by the large DLR feedback (e.g., Andrews et al., 2009).

An increase in surface temperature both warms and moistens the boundary layer through fast acting turbulent energy fluxes, so a surface warming will always be associated with a positive DLR response. This

constitutes a feedback between Earth's surface and the atmosphere that is not accounted for in "offline" experiments using land surface or sea ice model simulations that decouple DLR from surface temperature. In particular, offline or "land-only" simulations have been used to create soil moisture data proxies (e.g., Rodell et al., 2004; Zhao & Dirmeyer, 2003) and to investigate the impacts of land use change on the global climate (Lawrence et al., 2016). The cloud component of the DLR response that cannot be directly attributed to surface temperature changes with the radiative kernels constitutes a relatively small fraction of the full-sky response to greenhouse warming in our model ensemble. Therefore, a more accurate offline surface forcing would include the independent radiative forcing of clouds while accounting for the DLR response to surface temperature.

In conclusion, we stress that DLR and surface temperature anomalies are tightly coupled. Studies using uncoupled land and sea ice models frequently consider DLR an independent component of the surface energy budget; this fails to account for the influence of surface temperature on DLR highlighted in this paper. The assumption that DLR is an independent forcing on the surface is particularly prevalent in studies of land-atmosphere interaction and arctic climate, where surface temperature anomalies are frequently ascribed to enhancements in DLR. While DLR anomalies can certainly drive surface warming, the forcing and the response are difficult to distinguish because of the short equilibration timescale. We argue that surface temperature anomalies will always be associated with DLR anomalies through efficient boundary layer mixing and that surface temperature can exert a large influence on DLR through a strong lower atmosphere feedback. Any argument that DLR is driving surface temperature must carefully consider the origin of both anomalies, along with the certainty that any surface warming will generate a large DLR response.

Appendix A: Kernel Equations

The clear-sky surface kernels used in this analysis are adopted from Previdi (2010). For the traditional method, we simply multiplied changes in the model output at each location (x,y,p) with its corresponding kernel value. For the vertically integrated method, we assumed vertically invariant changes in temperature and specific humidity equal to the changes modeled at the surface. The surface radiative kernels have their largest weighting in the boundary layer, so the vertically integrated method yields results that are relatively insensitive to the level through which the surface perturbations are assumed to penetrate (see supporting information Figure S3). We chose to sum the entire column, but any upper integration limit above the boundary layer (850 hPa) gives a very similar answer.

In the traditional method, the temperature component ($\Delta\mathrm{DLR}_T$) at each grid box is given by

$$\Delta\mathrm{DLR}_T = \sum_k K_k^T \Delta T_k \quad . \tag{A1}$$

The subscript k represents vertical pressure levels and K_k^T indicates the temperature kernel value at the pressure level k. In the vertically integrated method, the temperature component is given by

$$\Delta\mathrm{DLR}_T = \Delta T_s \sum_k K_k^T \quad . \tag{A2}$$

Here, the subscript s represents a surface value.

Rather than a simple difference in specific humidity, the water vapor component in both methods is multiplied by the difference in $\ln q$. In the traditional method, the specific humidity component ($\Delta\mathrm{DLR}_q$) at each grid box is given by

$$\Delta\mathrm{DLR}_q = \sum_k K_k^q \Delta \ln q_k \quad . \tag{A3}$$

Similar to equation (A1), K_k^q is the specific humidity kernel value at pressure level k. In the vertically integrated method, the surface specific humidity component is given by

$$\Delta\mathrm{DLR}_q = \Delta \ln q_s \sum_k K_k^q \quad . \tag{A4}$$

To isolate the cloud component, we define two separate impacts of clouds on surface DLR. First, clouds are nearly perfect blackbodies in the longwave, so an increase in cloud cover (particularly at lower atmospheric

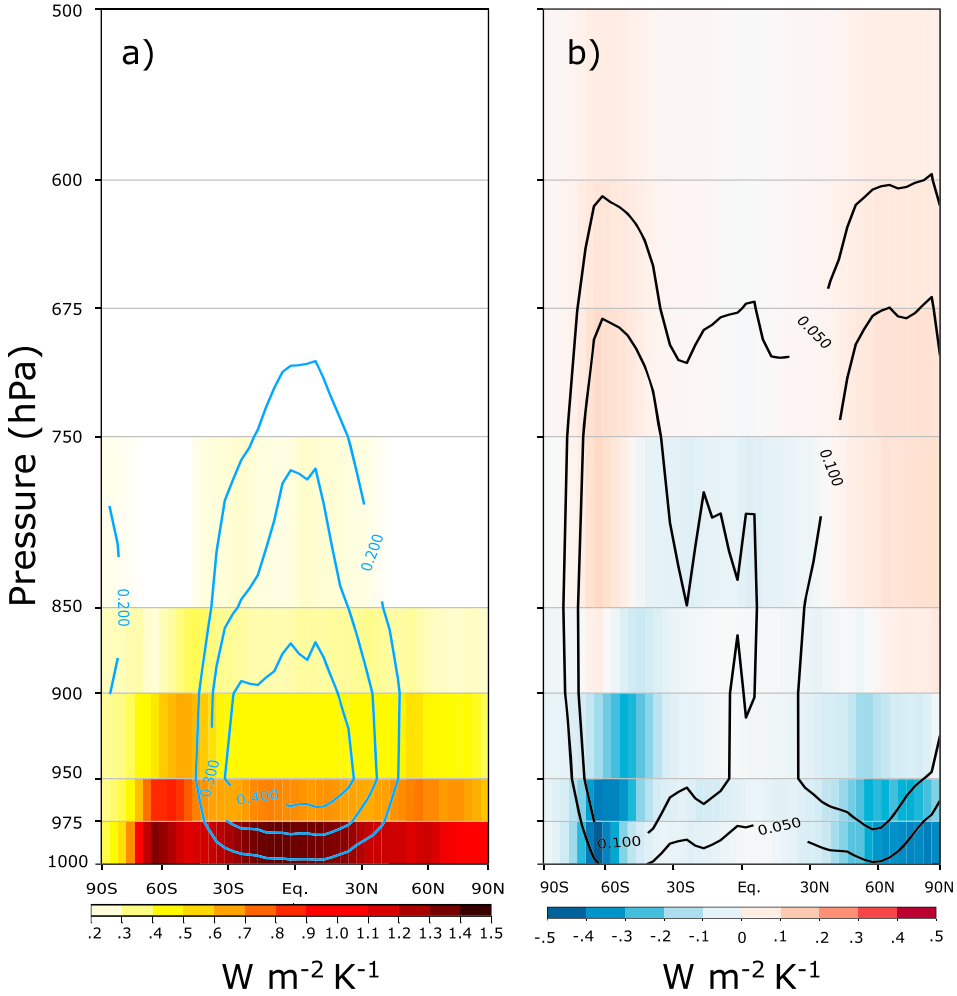

Figure A1. (a) Zonally averaged full-sky surface radiative kernels for temperature (shading) and specific humidity (contour interval 0.1 $W \cdot m^{-2} \cdot K^{-1}$) as a function of pressure level from Previdi (2010). The specific humidity kernel has been normalized such that values displayed show the longwave radiative change induced by the water vapor equivalent of a 1 K warming under the constant relative humidity assumption. (b) Differences between full- and clear-sky kernels (bracketed terms in equation (A5)). Colors show the difference between the two temperature kernels; contours show the difference between the two specific humidity kernels. The contour interval for the specific humidity kernel is $0.05 \frac{W}{m^2 \quad K}$, also note the color bar change for the temperature kernel.

levels) should have a positive impact on DLR; this is the cloud impact we would like to isolate. However, because clouds act as nearly perfect blackbodies, they also mask the temperature and humidity changes that occur above them. These masking effects are reflected in the different structures of the full-sky and clear-sky radiative kernels. To remove the effect of masking and thus properly estimate the true cloud component associated with changes in full-sky DLR, we start by subtracting the full-sky DLR from the clear-sky DLR and define this difference at $\Delta\bar{C}$, which includes both blackbody and masking impacts. Next, we use the full-sky and clear-sky kernels combined with the three-dimensional temperature and humidity fields to remove the effect of masking as follows:

$$\Delta C = \Delta\bar{C} - \sum_k \left[K_k^{T,c} - K_k^{T,f}\right] \Delta T_k - \sum_k \left[K_k^{q,c} - K_k^{q,f}\right] \Delta \ln q_k \quad . \tag{A5}$$

The c and f superscripts denote the clear- and full-sky kernels, respectively. Figure A1 shows the full-sky version of the kernels used in equation (A5) along with the difference between the full- and clear-sky kernels. Small though these differences are, they contribute to masking effects of clouds that we remove in our assessment of the cloud contribution to full-sky ΔDLR.

Acknowledgments
All climate model data were downloaded from the Earth System Grid Federation (ESGF) node hosted by Lawrence Livermore National Laboratory. The authors are grateful to all those who made the RCP8.5 modeling data open for public access, and to all the modeling groups who participated in the CMIP5 project. L. R. V. Z. was funded by NSF GRFP; A. D. was funded by NSF Antarctic Program Grant PLR 1643436; D. S. B. was funded by the Tamaki Foundation. The authors thank one anonymous reviewer for helpful comments.

References

Andrews, T., Forster, P. M., & Gregory, J. M. (2009). A surface energy perspective on climate change. *Journal of Climate*, *22*(10), 2557–2570. https://doi.org/10.1175/2008JCLI2759.1

Bony, S., Colman, R. C., Kattsov, V. M., Allan, R. P., Bretherton, C. S., Dufresne, J. l., et al. (2006). How well do we understand and evaluate climate change feedback processes? *Journal of Climate*, *19*(15), 3445–3482. https://doi.org/10.1175/JCLI3819.1

Burt, M. A., Randall, D. A., & Branson, M. D. (2016). Dark warming. *Journal of Climate*, *29*(2), 705–719. https://doi.org/10.1175/JCLI-D-15-0147.1

Colman, R. A. (2015). Climate radiative feedbacks and adjustments at the Earth's surface. *Journal of Geophysical Research: Atmospheres*, *120*, 3173–3182. https://doi.org/10.1002/2014JD022896

Feldl, N., & Roe, G. H. (2013). Four perspectives on climate feedbacks. *Geophysical Research Letters*, *40*, 4007–4011. https://doi.org/10.1002/grl.50711

Feldman, D. R., Collins, W. D., Gero, P. J., Torn, M. S., Mlawer, E. J., & Shippert, T. R. (2015). Observational determination of surface radiative forcing by CO_2 from 2000 to 2010. *Nature*, *519*, 339–343. https://doi.org/10.1038/nature14240

Hansen, J., Sato, M., Ruedy, R., Nazarenko, L., Lacis, A., Schmidt, G. A., et al. (2005). Efficacy of climate forcings. *Journal of Geophysical Research*, *110*, D18104. https://doi.org/10.1029/2005JD005776

Held, I. M., & Shell, K. M. (2012). Using relative humidity as a state variable in climate feedback analysis. *Journal of Climate*, *25*(8), 2578–2582. https://doi.org/10.1175/JCLI-D-11-00721.1

Held, I. M., & Soden, B. J. (2006). Robust responses of the hydrological cycle to global warming. *Journal of Climate*, *19*(21), 5686–5699. https://doi.org/10.1175/JCLI3990.1

Kim, H. M., & Kim, B. M. (2017). Relative contributions of atmospheric energy transport and sea ice loss to the recent warm Arctic winter. *Journal of Climate*, *30*(18), 7441–7450. https://doi.org/10.1175/JCLI-D-17-0157.1

Lawrence, D. M., Hurtt, G. C., Arneth, A., Brovkin, V., Calvin, K. V., Jones, A. D., et al. (2016). The Land Use Model Intercomparison Project (LUMIP) contribution to CMIP6: Rationale and experimental design. *Geoscientific Model Development*, *9*(9), 2973–2998. https://doi.org/10.5194/gmd-9-2973-2016

Mhyre, G., Shindell, D., Bréon, F. M., Collins, W., Fuglestvedt, J., Huang, J., et al. (2013). Climate change 2013: The physical science basis. Contribution of working group 1 to the fifth assessment report of the intergovernmental panel on climate change, Anthropogenic and Natural Radiative Forcing. Cambridge, United Kingdom and New York, NY: Cambridge University Press.

Pendergrass, A. G., Conley, A., & Vitt, F. (2018). Surface and top-of-atmosphere radiative feedback kernels for CESM-CAM5. *Earth System Science Data; Katlenburg-Lindau*, *10*(1), 317–324. https://doi.org/10.5194/essd-10-317-2018

Previdi, M. (2010). Radiative feedbacks on global precipitation. *Environmental Research Letters*, *5*(2), 025211. https://doi.org/10.1088/1748-9326/5/2/025211

Rodell, M., Houser, P., Jambor, U., & Gottschalck, J. (2004). The global land data assimilation system. *Bulletin of the American Meteorological Society*, *85*(3), 381–394. https://doi.org/10.1175/BAMS-85-3-381

Shell, K. M., Shields, J. T., & Shields, C. A. (2008). Using the radiative kernel technique to calculate climate feedbacks in NCAR's community atmospheric model. *Journal of Climate*, *21*(10), 2269–2282. https://doi.org/10.1175/2007JCLI2044.1

Soden, B. J., & Held, I. M. (2006). An assessment of climate feedbacks in coupled ocean-atmosphere models. *Journal of Climate*, *19*(14), 3354–3360. https://doi.org/10.1175/JCLI3799.1

Soden, B. J., Held, I. M., Coleman, R. C., Shell, K. M., Kiehl, J. T., & Shields, C. A. (2008). Quantifying climate feedbacks using radiative kernels. *Journal of Climate*, *21*(14), 3504–3520. https://doi.org/10.1175/2007JCLI2110.1

Stephens, G. L., Li, J., Wild, M., Clayson, C., Loeb, N., Kato, S., et al. (2012). An update on Earth's energy balance in light of the latest global observations. *Nature Geoscience*, *5*(10), 691–696. https://doi.org/10.1038/NGEO1580

Wild, M., Folini, D., Schär, C., Loeb, N., Dutton, E., & König-Langlo, G. (2013). The global energy balance from a surface perspective. *Climate Dynamics*, *40*(11), 3107–3134. https://doi.org/10.1007/s00382-012-1569-8

Woods, C., & Caballero, R. (2016). The role of moist intrusions in winter arctic warming and sea ice decline. *Journal of Climate*, *29*(12), 4473–4485. https://doi.org/10.1175/JCLI-D-15-0773.1

Zhao, M., & Dirmeyer, P. A. (2003). Production and analysis of GSWP-2 near-surface meteorology data sets (*COLA Tech. Rep. 159*). California.